Paper 88-2230, AIAA/ASME/ASCE/AHS 29th Structures, Structural Dynamics, and Materials Conf., Williamsburg, VA, April 18-20, 1988

DYNAMIC CHARACTERIZATION OF STRUCTURES BY PULSE PROBING AND DECONVOLUTION

A. S. Carasso*
E. Simiu**
National Bureau of Standards
Gaithersburg, Maryland

Abstract

This paper outlines the mathematical and computational basis of a procedure for identifying the dynamic behavior of linear structural systems from measurements of transient responses to specified pulses. The dynamic behavior of such systems is fully characterized by dynamic Green's functions, which can be reconstructed by deconvolution from response measurements. The deconvolution involves the solution of an ill-posed integral equation and can be performed by considering an associated Cauchy problem for a partial differential equation in which the measured response is used to define the initial condition. The explosive growth of errors due to contamination of the response by noise is prevented by regularizing the problem so as to minimize a Tikhonov functional. It is shown that infinitely divisible pulses, which include as a particular case the inverse Gaussian pulse, have properties which make it possible to perform continuous deconvolutions and to obtain bounds on errors induced by noise. The effectiveness of the proposed algorithm for reconstructing Green's functions is demonstrated in examples involving dispersive and nondispersive members, and a dispersive structural network that may be representative of a large space structure.

Nomenclature

a	wave propagation velocity (Eq. 29)
A_i	coefficients in Eq. 24
b	response to pulse excitation
b_n	response contaminated by noise
b_{nf}	filtered response data
EI	bending stiffness
g	dynamic Green's function
g_e	Green's function with error due to noise
GA_s	shear stiffness
$H(t)$	Heaviside unit step function
JG_1	torsional stiffness
ℓ	length
m	positive integer
M	bending moment
m_o	mass of hub
$n(t)$	noise
$p(t)$	pulse
s	variable in Laplace transform domain
t	time
T	torsional moment
V	shear force
w	deflection
x	space coordinate
$\{y\}$	state variable vector
β	parameter defining noise distribution
$\delta(t)$	Dirac delta function
ϵ	positive constant (Eq. 13)
ζ	argument in solution of wave equation
η	constant defining hysteretic damping
θ	angular deformation due to torsion
λ	eigenvalues
μ	constant (Eq. 14)
ξ	parameter in Fourier transform space
ρA	mass of beam per unit length
ρI	mass moment of inertia per unit length
$\rho_1 J$	mass moment of inertia about member axis
σ	parameter in inverse Gaussian pulse
τ	time parameter (Eq. 1)
ψ	angular deformation due to bending
ω	regularization parameter (Eq. 15)

Introduction

It has been pointed out that operating criteria governing automated functions of large space structures, such as directional orientation and figure maintenance, can be met only with distributed active controls[1]. For the controls to be effective, accurate information on the dynamic response of the structure must be available. This is also true of other flexible structures subjected to active controls (e.g., robot arms with noncollocated actuators and sensors[2]). The identification of dynamic properties is therefore essential in such applications.

Owing to the difficulties of earthbound dynamic testing and to the possibility that mechanical properties will change in flight as a result of environmental effects[3], it is desirable to test the structure dynamically in service (on orbit). Dynamic testing can be performed by exciting the structure harmonically over a range of frequencies, and recovering the natural frequencies of vibration and the modal damping parameters from the analysis of the corresponding set of steady state responses. However, under service conditions this method might be impractical; it is desirable to extract the dynamic information being sought in one fell swoop. Since the dynamic Green's function fully characterizes dynamic behavior, this can be done by exciting the structure with an appropriate pulse and extracting the dynamic Green's function of interest from the corresponding transient response.

This paper summarizes recent and current work performed at the National Bureau of Standards concerning mathematical and computational aspects of such a procedure. Reconstructing the dynamic Green's function from the measured response to a

* Research Mathematician, Center for Applied Mathematics
**NBS Fellow, Center for Building Technology

pulse entails the solution of an ill-posed integral equation in the presence of noise. We first describe briefly the mathematical basis of an algorithm for obtaining such a solution. To check its effectiveness, we apply the algorithm to noisy synthetic response data for structures whose exact dynamic Green's functions are known. These structures include a dispersive medium consisting of a Timoshenko beam, a nondispersive medium consisting of a slider with elastic deformations due to shear strain, and a network consisting of torsional members and Timoshenko beams. It is shown that the proposed algorithm results in reconstructed dynamic Green's functions that, for practical purposes, closely approximate their exact counterparts.

We note that research is also being conducted at the National Bureau of Standards on experimental aspects of the procedure described earlier. Currently work is proceeding on the development of a space-rated actuator capable of producing mathematically specified short mechanical pulses to be used for dynamic system identification purposes.

Inverse Gaussian Pulse Probes and Deconvolution of Response

The excitation, denoted by p(t), must be a smooth causal pulse of short duration which -- to an appropriate scale -- satisfies the relation

$$\int_0^\infty p(\tau)d\tau = 1 \tag{1}$$

We may refer to p(t) as a probability density function.

The response to the pulse p(t),

$$b(t) = \int_0^t p(t-\tau)g(\tau)d\tau \qquad 0 < t < \infty \tag{2}$$

will be in general a highly distorted image of the Green's function g(t), with the high frequency components smoothed out. (This will be illustrated by examples presented in the sequel.) The practical problem is to reconstruct the dynamic Green's function g(t) from the measured noisy response $b_n(t)$, since the response b(t) that would have been recorded in the absence of noise is unknown. Little is known about such problems in general. However, when the p(t) is infinitely divisible (i.e., for each integer m, p(t) is the m-fold convolution of another probability density defined on the positive axis), such problems have been intensively studied recently, both mathematically and computationally[4,5].

We first assume that the response is not contaminated by noise. To obtain g(t) from Eq. 2 we consider the Cauchy problem for the following linear partial differential equation in x, t:

$$\frac{\partial u}{\partial x} = \mathcal{F}^{-1}[\tilde{u}(\xi)\log(\sqrt{2\pi}\,\tilde{p}(\xi))] \qquad x > 0, \quad t > 0 \tag{3}$$

$$u(x,0) = 0, \qquad x > 0$$

$$u(0,t) = g(t) \qquad t > 0,$$

the Fourier transform of the causal signal f(t) being defined as

$$\mathcal{F}[f(t)] = \tilde{f}(\xi) = \frac{1}{\sqrt{2\pi}}\int_0^\infty f(t)e^{-i\xi t}\,dt \tag{4}$$

Fourier transformation of the first of Eqs. 3 yields an ordinary differential equation in $\tilde{u}(x,\xi)$ whose solution, by virtue of the third of Eqs. 3, is

$$\tilde{u}(x,\xi) = [\sqrt{2\pi}\,\tilde{p}(\xi)]^x\,\tilde{g}(\xi) \tag{5}$$

We take the inverse Fourier transform of Eq. 5 in which we set x = 1. The convolution theorem then yields

$$u(1,t) = \int_0^t p(t-\tau)g(\tau)d\tau \tag{6}$$

From Eqs. 2 and 6 it follows that we can obtain g(t) by integrating Eq. 3 from x = 1 to x = 0 and using b(t) as initial data on x = 1.

We now consider the important particular case in which the kernel is the inverse Gaussian pulse

$$p(\sigma,t) = \frac{\sigma H(t)}{\sqrt{4\pi t^3}}\exp(-\sigma^2/4t) \tag{7}$$

A moment pulse equal to $0.01p(\sigma,t)$ N m, with σ^2 = 0.04 seconds, is represented in Fig. 1.

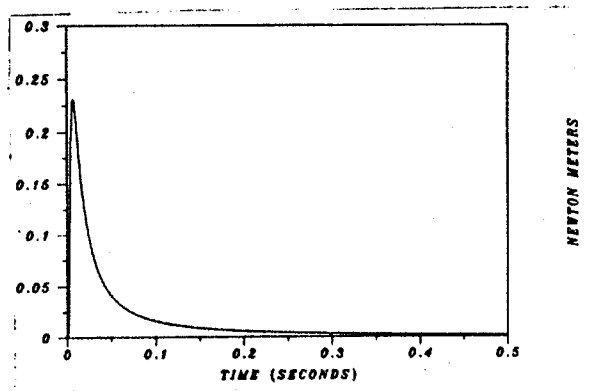

Fig. 1 Inverse Gaussian Pulse

The Laplace transform of Eq. 7 is

$$\mathcal{L}[p(\sigma, t)] = \exp(-\sigma s^{1/2}), \qquad \mathrm{Re}\ s > 0 \tag{8}$$

Therefore

$$p(\sigma_1,t) * p(\sigma_2,t) = p(\sigma_1 + \sigma_2,t) \tag{9}$$

and we can write Eq. 2 in the form

$$b(t) = p(\sigma,t) * g(t)$$

$$= p(\frac{\sigma}{m}, t) * [p(\frac{\sigma}{m}, t)]^{*(m-1)} * g(t) \tag{10}$$

The step by step marching procedure of the Cauchy problem corresponds to solving Eq. 10 by successively removing the narrow convolution factors $p(\sigma/m, t)$ from its right-hand side. We refer to this procedure, which allows the monitoring of the unsmoothing process from u(1, t) = b(t) to u(0, t) = g(t) as continuous deconvolution.

As indicated previously, in practice the response data are contaminated by noise, so that

instead of Eq. 2 we have

$$b_n(t) = \int_0^t p(\tau, t-\tau) g_e(\tau) d\tau \qquad 0 < t < \infty \qquad (11)$$

where $g_e(\tau)$ is an estimate of the Green's function as affected by errors due to the unknown noise

$$n(t) = b_n(t) - b(t) \qquad (12)$$

whose norm is assumed to satisfy

$$\int_0^\infty n^2(t)dt \leq \epsilon^2 \qquad (13)$$

We also assume that there exists a positive constant μ such that

$$\int_0^\infty g^2(t)dt \leq \mu^2 \qquad (14)$$

The ratio

$$\omega = \frac{\epsilon}{\mu} \ll 1 \qquad (15)$$

is the root mean square of the noise-to-signal ratio in $b_n(t)$.

Laplace transformation of Eq. 11 yields

$$\exp(-\sigma s^{1/2}) G_e(s) = B(s) + N(s) \qquad (16)$$

where the notation F(s) is used for the Laplace transform of f(t). On the other hand

$$\exp(-\sigma s^{1/2}) G(s) = B(s) \qquad (17)$$

It can then be shown by using the Schwarz inequality that

$$\frac{|G_e(s) - G(s)|}{|G_e(s)|} \geq \frac{\sqrt{2\mathrm{Re}\ s}}{\mu} |e^{\sqrt{\sigma s}}| |N(s)| \qquad (18)$$

i.e., for large values of s the noise can result in enormous relative errors in $G_e(s)$. Therefore, using the measured response $b_n(t)$ as initial data on $x = 1$ can cause the solution to be drowned in spurious oscillations to the extent of rendering it useless for practical purposes. This is illustrated in the following section for the case of the Timoshenko beam.

It is therefore necessary to regularize the solution by appropriately filtering the data. It is shown in[4] that, to obtain the approximation to g(t) that minimizes the Tikhonov functional associated with Eq. 11[6,7], it is necessary to replace the Fourier transform of the initial data on $x = 1$, $\tilde{b}_n(\xi)$, by the filtered data

$$\tilde{b}_{nf}(\xi) = \frac{|\tilde{p}(\xi)|^2 \tilde{b}_n(\xi)}{|\tilde{p}(\xi)|^2 + (\omega^2/2\pi)} \qquad (19)$$

The choice of ω in Eq. 19 is determined by information on the approximate noise level inherent in the measurements being performed, and on information of experimental or analytic origin on the approximate time dependence of the dynamic Green's function. Numerical experimentation using interactive graphics is then quite effective in locating the optimal value of ω.

The property of infinite divisibility allows the calculation of error bounds for the dynamic Green's functions being reconstructed (see[5,8] for details).

Applications

The purpose of the applications presented in this section is to demonstrate the effectiveness of the proposed algorithm for reconstructing dynamic Green's functions from noisy responses to infinitely divisible pulses. We confine ourselves in this paper to inverse Gaussian pulses (Eq. 7) which, as seen in Fig. 1, are unimodal. A rich variety of infinitely divisible pulses can be constructed[5], which can be useful for modeling distortions, superimposed small oscillations, deviations from a prescribed shape, and other perturbations due to the instrumentation. Applications of the theory of multimodal pulses to the structural dynamics identification problem will be presented in a forthcoming paper.

The noisy response $b_n(t)$ is constructed as follows. We first calculate the dynamic Green's function g(t) for the member or system being considered. We then use Eq. 2 to calculate the response b(t). The response $b_n(t)$ is created synthetically by adding noise, n(t), to b(t). For any given t, the noise (perturbation) n(t) is a random number drawn from a uniform distribution in the range $\pm \beta b(t)$. For example, if $\beta = 0.01$, we refer to the perturbation as "1% noise".

Given the noisy response $b_n(t)$, we reconstruct the dynamic Green's function by using the algorithm based on the solution of the regularized Cauchy problem associated with Eq. 11. Details of the algorithm are given in[5].

Simply Supported Timoshenko Beam.

Dynamic Green's Function. We seek the dynamic Green's function for the slope at $x = \ell$ of the Timoshenko beam with the loading and support conditions shown in Fig. 2. The equations of motion of the beam are[9]

$$\frac{\partial V}{\partial x} = \rho A \frac{\partial^2 w}{\partial t^2}, \quad \frac{\partial M}{\partial x} - V = \rho I \frac{\partial^2 \psi}{\partial t^2} \qquad (20)$$

with the constitutive relations

$$M = EI \frac{\partial \psi}{\partial x}, \qquad V = GA_s \frac{\partial w}{\partial x} + \psi \qquad (21)$$

The state variable vector is defined as

$$\{y\} = \{-w, \psi, M, V\}^T \qquad (22)$$

Fourier transformation of Eqs. 20-21 yields

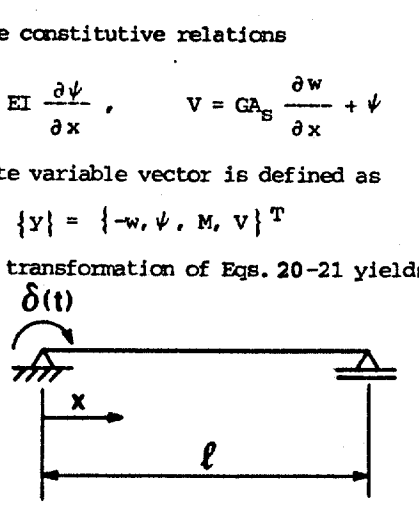

Fig. 2 Simply Supported Timoshenko Beam

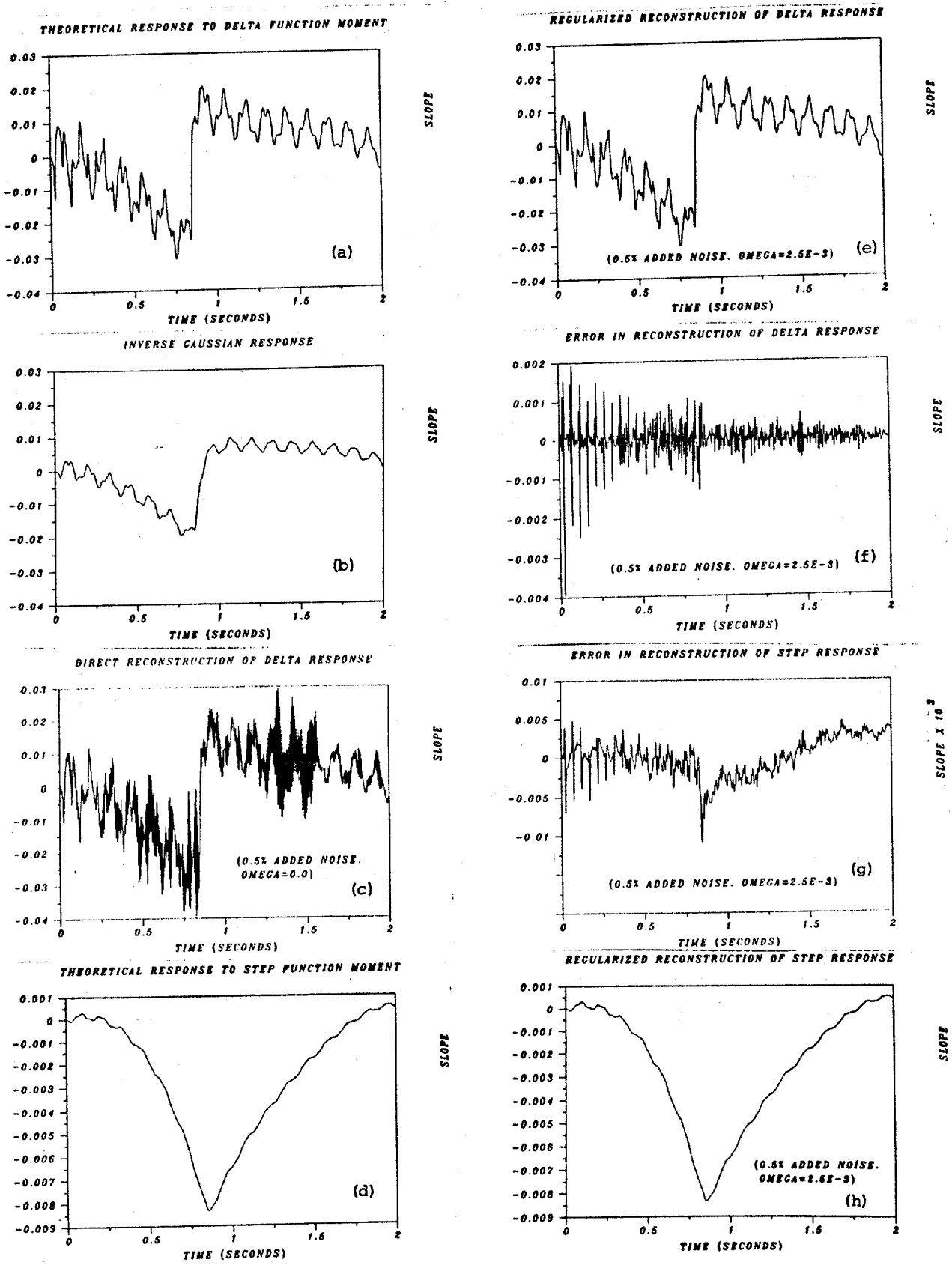

Fig. 3 Results Obtained for Timoshenko Beam

$$\left\{\frac{d\tilde{y}}{dx}\right\} = \begin{bmatrix} 0 & 1 & 0 & -1/GA_s \\ 0 & 0 & 1/EI & 0 \\ 0 & -\rho I\xi^2 & 0 & 1 \\ \rho A\xi^2 & 0 & 0 & 0 \end{bmatrix} \{\tilde{y}\} \qquad (23)$$

The general solution for V is[10]

$$\tilde{V} = A_1\cosh(\lambda_1 x/\ell) + A_2\sinh(\lambda_1 x/\ell) + A_3\cos(\lambda_2 x/\ell) + A_4\sin(\lambda_2 x/\ell) \qquad (24)$$

($\pm\lambda_1$ and $\pm i\lambda_2$ are the eigenvalues of the matrix in Eq. 23; note that λ_1 and λ_2 are functions of ξ.) The general solutions for the other components of the state vector follow immediately from the Fourier transforms of Eqs. 20 and 21.

The boundary conditions are

$$w = 0\ ;\quad M = 0.01\delta(t)\ \text{Nm} \quad \text{at } x = 0 \qquad (25)$$
$$w = 0\ ;\quad M = 0 \quad \text{at } x = \ell$$

The slope at $x = \ell$ is

$$\left.\frac{\partial\tilde{w}}{\partial x}\right|_{x=\ell} = \frac{-1}{\rho A\xi^2\ell^2}\left[A_1\lambda_1{}^2\cosh\lambda_1 + A_2\lambda_1{}^2\sinh\lambda_1 - A_3\lambda_2{}^2\cos\lambda_2 + A_4\lambda_2{}^2\sin\lambda_2\right] \qquad (26)$$

It follows from the boundary conditions that

$$A_4 = -A_2\frac{1}{\lambda_2} \qquad (27)$$

$$A_1 = \frac{1}{\sinh\lambda_1}\left[-A_2(\cosh\lambda_1 - \cos\lambda_2) + A_3\frac{\lambda_2\sin\lambda_2}{\lambda_1}\right]$$

$$A_3 = -A_2\frac{1}{\lambda_2\tan\lambda_2}$$

$$A_2 = \frac{\rho A\xi^2\ell^3}{\lambda_1(\lambda_1{}^2 + \lambda_2{}^2)EI}$$

The dynamic Green's function being sought is the inverse Fourier transform of Eq. 26.

Calculations were performed assuming the following values for the parameters of the beam: $\rho A = 0.425$ kg/m, $\rho I = 2.78 \times 10^{-4}$ kgm, $EI = 0.555(1 + i\eta\,\mathrm{sgn}\xi)$ Nm^2, $GA_s = 0.711(1 + i\eta\,\mathrm{sgn}\xi)$ N, $\ell = 1.1$ m, $\eta = 0.01$. (These values were calculated in[11] in an attempt to obtain an equivalent Timoshenko rotating beam whose response would match the measured response of a flexible robot arm[2].) The calculated dynamic Green's function is shown in Fig. 3a for $0 < t < 2$ s. It is noted that the Timoshenko beam, whose motion is governed by a fourth order partial differential equation, is a dispersive medium.

Numerical Reconstruction of Dynamic Green's Function From Noisy Response. The slope at $x = \ell$ due to an inverse Gaussian pulse with $\sigma = 0.2$ s$^{1/2}$ (Fig. 1) acting at $x = 0$ is obtained from Eq. 2 and is shown in Fig. 3b. The response is seen to be a distorted image of the dynamic Green's function (Fig. 3a), with high frequency components smoothed out. We add 0.5% noise to the response at each of 720 equidistant points in the interval [0, 2] s.

Direct reconstruction of the Green's function from noisy data is shown in Fig. 3c. Note the strong amplification, typical of ill-posed problems, of the small amount of noise in the data. The regularized reconstruction with $\omega = 2.5 \times 10^{-3}$, shown in Fig. 3e, is a great improvement over the direct reconstruction. Note, however, that sharp features in the early part of the response have been rounded by the reconstruction algorithm. Figure 3f shows the errors in the reconstruction (i.e., the differences between the original and the reconstructed Green's function). The largest errors occur in the early part of the signal and are due to the minute rounding mentioned above.

Recall that dynamic Green's functions are used to calculate the response to physically realizable (i.e., smooth) loadings by convolution, as in Eq. 2. The errors in the reconstructed Green's function will cause errors in the calculated response. However, owing to the averaging action of the integration process, these errors will be considerably smaller than those affecting the reconstructed Green's function. To illustrate the favorable effect of integration, we consider the slope of the beam at $x = \ell$ due to the step moment $0.01H(t)$. Figures 3d and 3h show the step response calculated by convolution of the step function with the kernel consisting of the original and the reconstructed Green's function, respectively. The agreement between the two responses is much closer than is the case for the corresponding Green's functions. This is also seen in Fig. 3g, which shows the errors in the regularized step response. The maximum absolute error occurs near the middle of the interval and is of the order of 0.1% of the corresponding ordinate of the response.

Mechanical Slider With Deformations Due To Shear Stress.

Dynamic Green's Function. The equations of motion and the constitutive relations for this member, depicted in Fig. 4, are

$$\frac{\partial V}{\partial x} = \rho A\frac{\partial^2 w}{\partial t^2}\ ,\quad \frac{\partial w}{\partial x} = \frac{V}{GA_s} \qquad (28)$$

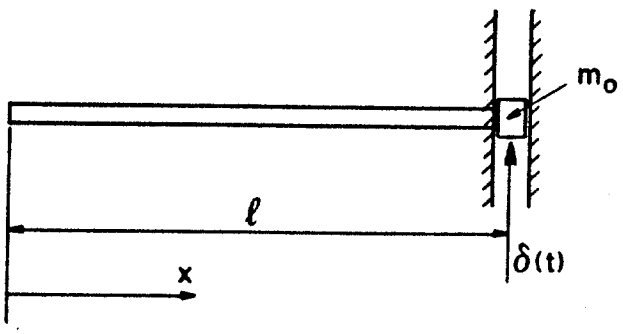

Fig. 4 Mechanical Slider

so that

$$\frac{\partial^2 w}{\partial t^2} = a^2 \frac{\partial^2 w}{\partial x^2} \qquad (29)$$

$$a^2 = \frac{GA_s}{\rho A}$$

The boundary conditions are

$$V = 0 \quad \left(\text{or } \frac{\partial w}{\partial x} = 0\right) \quad \text{for } x = 0 \qquad (30)$$

$$m_o \frac{\partial^2 w}{\partial t^2} = -\delta(t) - V \quad \text{for } x = \ell \ .$$

Note that the motion of the slider is governed by the wave equation. Unlike the Timoshenko beam the slider is therefore a nondispersive medium. The general solution of Eq. 29 is

$$w = f(at - x) + F(at + x) \qquad (31)$$

The first boundary condition yields

$$w = f(at - x) + f(at + x) \qquad (32)$$

To obtain the functional form of $f(\zeta)$ [the argument ζ may be put equal to at - x or at + x as required], we note that the second of Eqs. 30 is a condensed form of the boundary condition

$$\frac{m_o}{\rho A} \frac{\partial^2 w}{\partial t^2} = -a^2 \frac{\partial w}{\partial x} \quad \text{for } x = \ell \qquad (33)$$

and the initial conditions

$$w = 0 \quad \text{for } t = 0 \text{ and } 0 < x < \ell \qquad (34)$$

$$\lim_{t=+0} \frac{\partial w}{\partial t} = -\frac{1}{m_o} \quad \text{for } x = \ell$$

As shown for an entirely analogous problem in[12], the first of Eqs. 34 implies

$$\frac{\partial w}{\partial x} = 0 \text{ and } \frac{\partial w}{\partial t} = 0 \quad \text{for } t = 0;\ 0 < x < \ell \qquad (35)$$

Equations 35, and the first of Eqs. 34 for x = 0, yield

$$f(\zeta) = 0 \qquad -\ell < \zeta < \ell \qquad (36)$$

To obtain the expression of $f(\zeta)$ for the interval $\ell < \zeta < 3\ell$ we use Eq. 33, which provides the "continuing equation", the second of Eqs. 34, and the condition that there is no sudden change in the displacement at $x = \ell$. The result is

$$f(\zeta) = -\frac{1}{a\rho A}\left[1 - \exp\left[-\frac{\rho A}{m_o}(\zeta - \ell)\right]\right] \qquad (37)$$

The expressions of $f(\zeta)$ for successive intervals $(2k-1)\ell < \zeta < (2k+1)\ell$, where k = 2, 3,..., are obtained recursively using the continuing equation, the condition of continuity of the velocity at $x = \ell$, and the condition that there is no sudden change in the displacement at $x = \ell$. The dynamic Green's function of the acceleration at $x = \ell/7$, derived from Eq. 32 in which the appropriate expressions for $f(\zeta)$ were used, is shown in Fig. 6a for $m_o = 0.225$ kg, $\rho A = 0.425$ kg/m, and $GA_s = 0.711$ N. The Green's functions for the velocity and displacement at $x = \ell/7$ are shown in Figs. 6b and 6c, respectively.

Numerical Reconstruction of Dynamic Green's Function From Noisy Response. The acceleration response at $x = \ell/7$ due to an inverse Gaussian pulse with $\sigma = 0.5\ s^{1/2}$ acting at $x = \ell$ is shown in Fig. 5. The response is seen to be a highly distorted image of the corresponding Green's function (Fig. 6a). Next 1% noise was added to this response. The

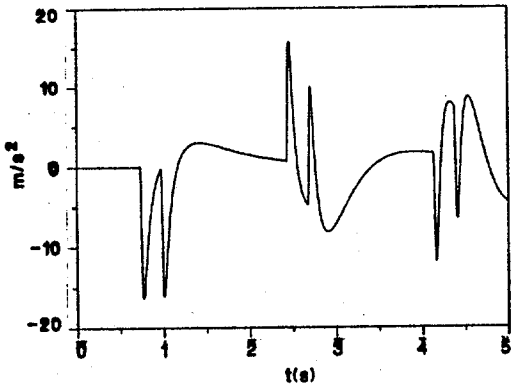

Fig. 5 Acceleration Due to Inverse Gaussian Pulse

dynamic Green's function, reconstructed from the noisy response to the pulse using the regularization parameter $\omega = 1.0 \times 10^{-4}$, is shown in Fig. 6d. The reconstructed Green's function has less sharp peaks than its exact counterpart, and it is also affected by spurious high-frequency components. Note that the accuracy of the reconstruction would have been improved had a sharper pulse been used.

The reconstructed Green's function of the velocity at $x = \ell/7$ was obtained by integrating the reconstructed Green's function of the acceleration with respect to time. The result is shown in Fig. 6e. The agreement with the exact Green's function of the velocity (Fig. 6b) is much better than for the accelerations; as indicated earlier, integration considerably reduces errors due to deconvolution in the presence of noise. Integration of the reconstructed velocity (i.e., integrating the reconstructed acceleration twice) results in a reconstructed Green's function of the displacement (Fig. 6f) that is virtually indistinguishable from the corresponding exact Green's function (Fig. 6c).

Structural Network With Torsional Members and Timoshenko Beams.

The hypothetical space structure of Fig.7 consists of four identical torsional members (1-2, 1'-2', 2-3, 2'-3') and two Timoshenko beams (2-2' and 3-3'). The moment connections between the torsional members and the Timoshenko beams are rigid. The network and its impulsive loadings are symmetrical about the line joining the midpoints of the beams.

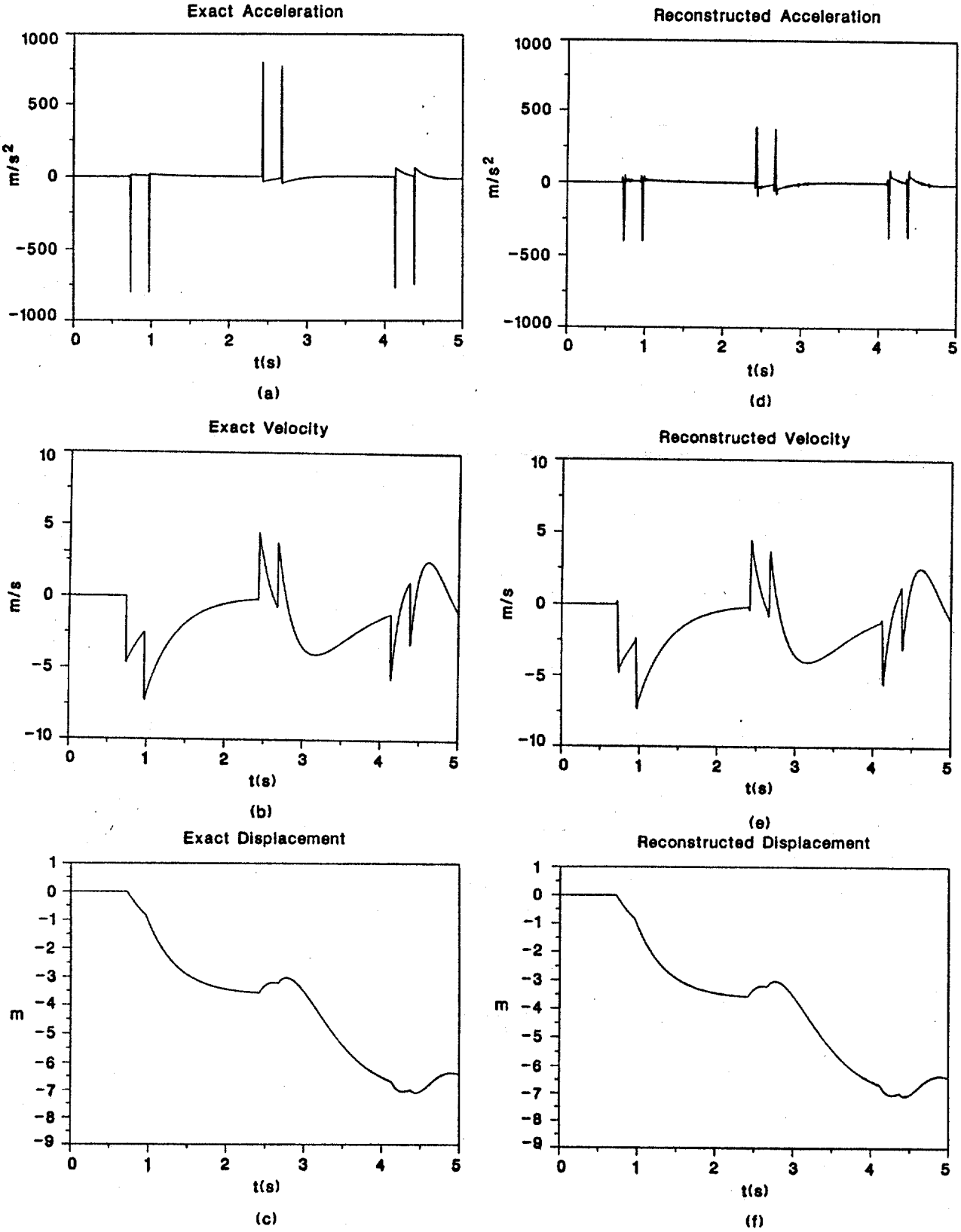

Fig. 6 Results Obtained for Mechanical Slider

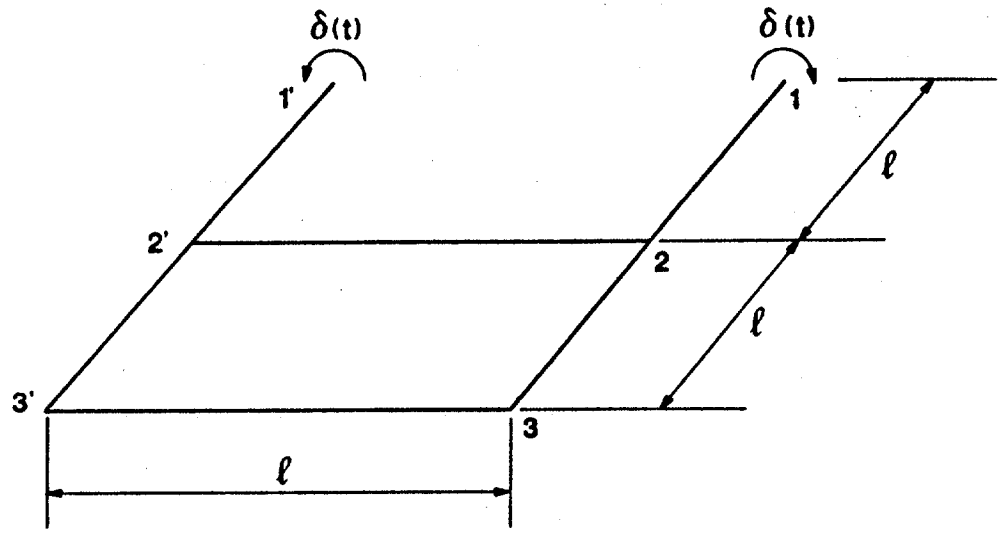

Fig. 7 Structural Network (ℓ = 195 m)

The equation of motion and the constitutive equation for the torsional members are

$$\frac{\partial T}{\partial x} = \rho_1 J \frac{\partial^2 \theta}{\partial t^2} \; ; \quad \frac{\partial \theta}{\partial x} = \frac{T}{JG_1} \tag{38}$$

From the first of Eqs. 38 it follows that the general solution for the Fourier transform of the rotation of in each torsional member is of the form

$$\tilde{\theta}(x) = \tilde{\theta}(0)\cos\left(\frac{\lambda x}{\ell}\right) + \tilde{T}(0)\,\frac{\ell}{\lambda JG_1}\sin\left(\frac{\lambda x}{\ell}\right) \tag{39}$$

$$\lambda = \left[\frac{\rho_1 J}{JG_1}\right]^{1/2} \xi \ell \tag{40}$$

A similar relation is obtained for $\tilde{T}(x)$ from the second of Eqs. 38. The general solution for the Fourier transforms of the shear force in each beam is of the same form as Eq. 24. The general solutions for the Fourier transforms of the other components of the state vector (-w, ψ , and M) follow from Eq. 24 and the Fourier transforms of Eqs. 20 and 21.

There are altogether 16 unknown coefficients (two for each torsional member and four for each beam). The 16 requisite boundary conditions are the following: torques at joints 1 and 1' are equal to unity, i.e., to the Fourier transform of the applied torques (2 conditions); sum of torsional and bending moments at joints 2, 2',3, 3'are zero (4 conditions); shear forces at the ends of the beams are zero, since torsional members are assumed not to be capable of transmitting shear force (4 conditions); rotations of collinear torsional members at joints 2 and 2' are equal (2 conditions); rotations of torsional members and slopes of beams at joints 2, 2', 3, 3' are equal (4 conditions). Note that it is possible in this case to take advantage of symmetry, which allows the reduction of the number of unknowns to twelve. Once the unknown coefficients are determined as functions of the frequency parameter, the Green's function being sought is obtained by inverse Fourier transformation of the quantity of interest (e.g., rotation, slope, moment).

Calculations were performed for the following values of the network parameters (see[11], pp. 16-20): ρA = 2.39 kg/m; ρI = 11.8 kg m, EI = 1.77 x 10^8 (1 + $i\eta\,\mathrm{sgn}\xi$) N m^2, ℓ = 195 m, η = 0.001. The Green's function for the slope at joint 3 of beam 3-3' due to the moments impulses of Fig. 7 is shown in Fig. 8a. The disturbances consisting of the moment impulses at joints 1 and 1' propagate to joint 3 partly through the beams 3-3' and 2-2', which are dispersive. That is, the various frequency components of the disturbances, which were originally synthesized in a sharp signal, travel at different speeds and arrive at joint 3 at different times. The dispersion of the higher frequency components is evident in Fig. 8a. A similar dispersion occurs in the case of the Green's function shown in Fig. 3a. The higher the damping, the faster the high frequency components are smoothed out. This is seen by comparing the Green's functions for the slope of the beam at joint 2, calculated by assuming the hysteretic damping to be 0.1% on the one hand (Fig. 8a), and 1% on the other (Fig. 9). Finally, note the contrast between the Green's functions of Figs. 3a, 8a, and 9, which are typical of dispersive media, and the Green's functions for the nondispersive mechanical slider (Figs. 4a, b, c).

Numerical Reconstruction of Dynamic Green's Function From Noisy Response. Figure 8b shows the response obtained by convolving the Green's function of Fig. 8a and an inverse Gaussian pulse with σ = 0.2 $s^{1/2}$. The drastic smoothing out of the sharp features of the Green's function is evident. The noisy response was constructed by adding 1% noise to the response of Fig. 8b.

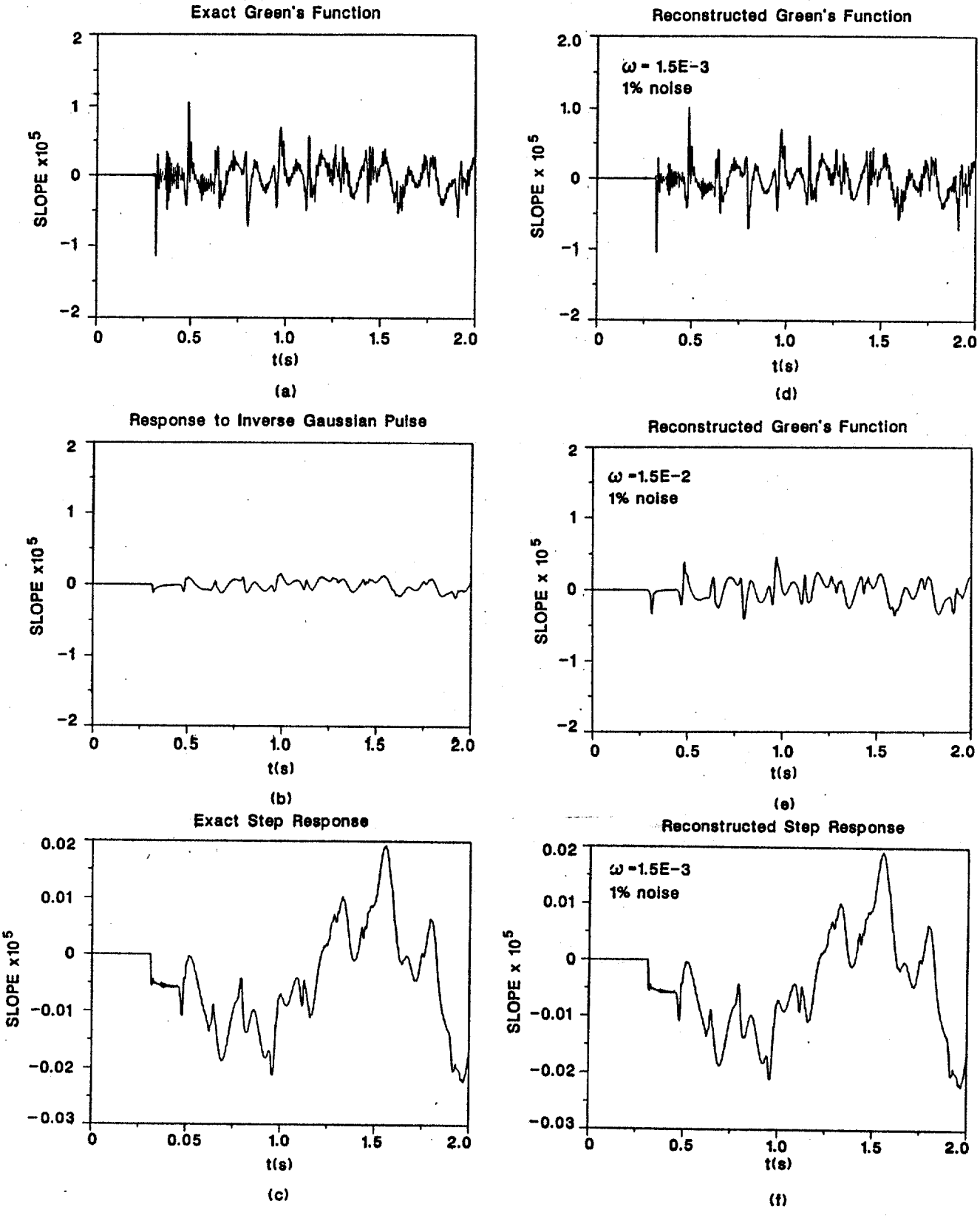

Fig. 8 Results Obtained for Structural Network, η = 0.001

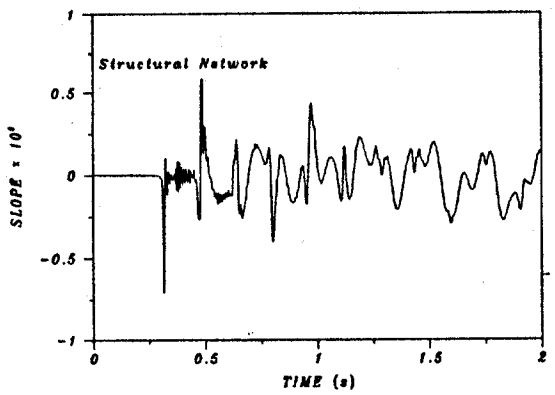

Fig. 9 Exact Green's Function, η = 0.01

The regularized reconstruction of the dynamic Green's function, using $\omega = 1.75 \times 10^{-3}$, is shown in Fig. 8d. Much of the detailed structure of the Green's function has been preserved, although a few discrepancies can be detected. However, the errors inherent in Fig. 8d are of little consequence when the reconstructed Green's function is used as a tool for predicting the response to a given smooth function f(t). Indeed, as pointed out earlier, small pointwise errors tend to be averaged out by the convolution process. As an example, the reconstructed step response (Fig. 8f) obtained by convolution of the unit step function with the reconstructed Green's function of Fig. 8d is virtually indistinguishable from the exact step response (Fig. 8c). It is noted that if the errors in the reconstructed Green's functions are large -- as may be the case in an unregularized (direct) reconstruction -- the convolution process may not be sufficiently effective in averaging them out.

To illustrate the importance of selecting the optimal value of the regularizing parameter, we show in Fig. 8e a reconstruction in which $\omega = 1.5 \times 10^{-2}$. Because this value is too large, it causes the smoothing out of legitimate high-frequency components of the signal.

For the case η = 0.01, Fig. 10 shows a view of 12 successive steps (see Eq. 10) in the reconstruction process that proceeds from the response to the pulse (first trace in foreground) to the Green's function being sought (last trace in background). Such diagrams, interpreted in the light of error bounds developed in[8], can be helpful in attempts to determine whether certain high-frequency components of a reconstructed Green's function belong legitimately to the signal or are spurious additions due to noise.

Additional details on various aspects of the work presented here are available in[13].

Conclusions

A mathematical and computational capability exists that would enable the reliable experimental determination of dynamic Green's functions for structures. The method is based on propagating specific types of pulses leading to a tractable deconvolution problem in the presence of noise.

Acknowledgments

This work was sponsored by the Directorate of Aerospace Sciences, Air Force Office of Scientific Research. Dr. Anthony K. Amos served as the project monitor. The Minerals Management Service, U.S. Department of the Interior (Charles E. Smith, Research Program Manager) also provided partial support.

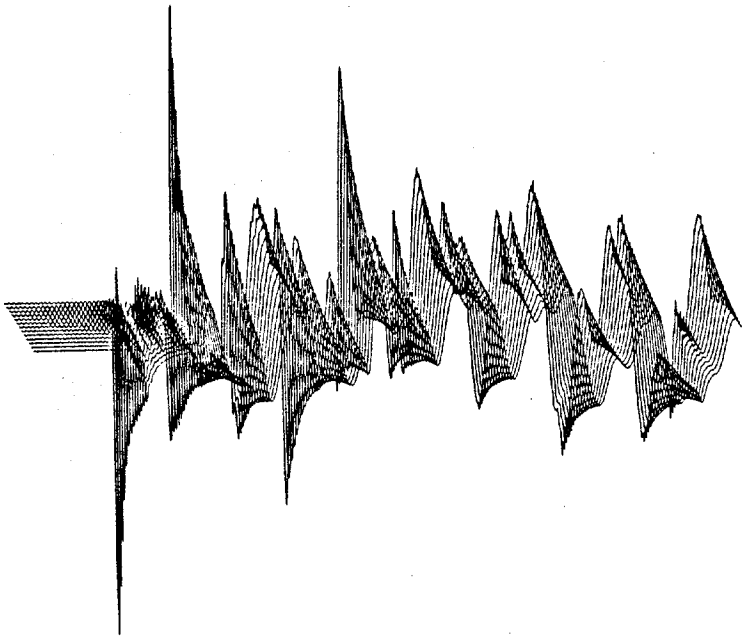

Fig. 10 View of Successive Partial Deconvolutions for Structural Network, η = 0.01

References

1. Ashley, H., "Some Considerations on Earthbound Dynamic Testing of Large Space Structures", Paper 86-0908, 27th Structures, Structural Dynamics, and Materials Conference, Part 2, San Antonio, Texas, May 19- 21, 1986, American Institute of Aeronautics and Astronautics, New York, N.Y., pp. 362-373.

2. Cannon, R. H. Jr., and Schmitz, E., "Initial Experiments on the End-Point Control of a Flexible One-Link Robot," The International Journal of Robotics Research, Vol. 3, No. 3, Fall 1984, pp. 62-75.

3. Crawley, E. F., and de Luis, J., "Use of Piezoelectric Actuators as Elements of Intelligent Systems," AIAA Journal, Vol. 25, Oct. 1987, pp. 1373-1385.

4. Carasso. A. S., and Hsu, N. N., "Probe Waveforms and Deconvolution in the Experimental Determination of Elastic Green's Functions," SIAM Journal on Applied Mathematics, Vol. 45, No. 3, June, 1985, pp. 369-382.

5. Carasso, A. S., "Infinitely Divisible Pulses, Continuous Deconvolution, and the Characterization of Linear Time Invariant Systems," SIAM Journal on Applied Mathematics, Vol. 47, No. 4, Aug. 1987, pp. 892-927.

6. Franklin, J. N., "On Tikhonov's Method for Ill-Posed Problems," Mathematics of Computation, Vol. 28, 1974, pp. 889-907.

7. Franklin, J. J., "Minimum Principles for Ill-Posed Problems," SIAM Journal on Mathematical Analysis, Vol. 8, 1978, pp. 638-650.

8. Carasso, A. S., and Hsu, N. N., "L^{∞} Errors in Partial Deconvolution of the Inverse Gaussian Pulse," SIAM Journal on Applied Mathematics, Vol. 45, No. 6, Dec. 1985, pp. 1029-1038.

9. Hurty, W. C., and Rubinstein, M. F., Dynamics of Structures, Prentice-Hall, Englewood Cliffs, N.J., 1964, p. 88.

10. Pestel, E. C., and Leckie, F. A., Matrix Methods in Elastomechanics, McGraw-Hill, New York, 1963, p. 133.

11. von Flotow, A. H., "Disturbance Propagation in Structural Networks; Control of Large Space Structures," Ph. D. Dissertation, Department of Aeronautics and Astronautics, Stanford University, June 1984.

12. Love, A. E. H., A Treatise on the Mathematical Theory of Elasticity, 4th ed. Dover, New York, 1944, p. 435.

13. Carasso, A. S., and Simiu, E., "Identification of Dynamic Green's Functions in Structural Networks," paper submitted for possible publication to the AIAA Journal.